

## A “Force Buffer” Protecting Immunoglobulin Titin\*\*

João M. Nunes, Ulf Hensen, Lin Ge, Manuela Lipinsky, Jonne Helenius, Helmut Grubmüller,\* and Daniel J. Muller\*

Titin filaments control structural and functional properties of the sarcomere.<sup>[1]</sup> They connect the M-line and Z-disc components of the sarcomere which are approximately 1  $\mu\text{m}$  apart. The sarcomere consists of four regions: the M-line, A-band, I-band, and Z-line. Most of titin's extensibility is credited to the I-band<sup>[2,3]</sup> which contains immunoglobulins (Igs) flanking N2 and PEVK regions. The N2 and PEVK regions behave like unstructured entropic springs and are easily extended.<sup>[4]</sup> The Ig domains of the I-band have the  $\beta$ -stranded fold of the Ig family.<sup>[5,6]</sup>

The mechanical unfolding of titin Ig has been extensively characterized by single-molecule force spectroscopy (SMFS).<sup>[7–10]</sup> The Igs of proximal and distal I-band regions unfold differently.<sup>[4]</sup> While proximal Igs unfold following a two-state model, distal Igs follow a three-state model.<sup>[4]</sup> I27, a distal Ig of titin, unfolds via an intermediate state when mechanically stressed.<sup>[7,8,11,12]</sup> The unfolding intermediate was suggested to form when the hydrogen-bond network between the  $\beta$ -strands A and B is ruptured while the rest of I27 remains folded.<sup>[8,12]</sup> Removal of  $\beta$ -strand A eliminates this unfolding intermediate and leaves the core stability of I27 unaltered.<sup>[13]</sup> Recent intriguing findings show that the force required to convert into the unfolding intermediate does not change with temperature while the force required for complete unfolding does.<sup>[14]</sup>

Using a I27 octamer (I27<sub>8</sub>), we show that the force of approximately 95 pN at which the I27 unfolding intermediate forms is largely independent of the force loading rate (applied force versus time). Thus, stressing forces  $\ll$  95 pN hardly

lower the energy barrier separating folded from intermediate state. Because I27 must unfold via this intermediate this force loading rate independency protects I27 from unfolding at low, physiologically relevant, stressing forces. Moreover, the combined contributions of all Igs within the distal region of the I-band may constitute a “force buffer” that protects titin from mechanical stress.

We applied SMFS to examine the unfolding of I27 in quasi-natural conditions. I27<sub>8</sub> molecules were covalently attached to gold surfaces through C-terminal cysteine residues. By lowering the cantilever tip onto the N-terminus of I27<sub>8</sub>, the N-terminus was non-specifically attached to the tip. The mechanical response of I27<sub>8</sub> was measured as the tip was withdrawn (Figure 1). I27s unfolded sequentially at stretching forces between 150–300 pN, resulting in a sawtooth patterned force–distance (F–D) curve (Figure 1a).<sup>[7]</sup> The unfolding of each I27 increases the length of the polypeptide by approximately 28 nm<sup>[8]</sup> and reduces the tension. As the tip is further withdrawn the force applied increases until the next I27 unfolds. We established an automatic routine (Supporting Information) to identify the unfolding peaks, including the transition to intermediate unfolding states, (“humps”) in F–D curves (Figure 1c).

Earlier SMFS studies of I27 were performed in PBS buffer (phosphate buffered saline solution) which mimics extracellular conditions. We characterized the unfolding of I27 in buffers that mimic the cytosol (Supporting Information). Both the force at which the unfolding intermediate formed and I27 unfolded completely did not depend on buffer used (Supporting Information, Figure S1).

An unfolding intermediate was observed in approximately 95% of the first unfolding peaks, regardless of how many I27s unfolded thereafter (Supporting Information, Figure S2). To reveal the structural transitions and interactions of the unfolding process, we performed atomistic force–probe molecular dynamics simulations (FPMD).<sup>[15,16]</sup> Since the F–D curves showed that the force of the unfolding intermediate was unaffected by the number of I27s (Supporting Information, Figure S3), we used the X-ray structure of monomeric I27 (protein data bank (PDB) code 1WAA)<sup>[17]</sup> for FPMD. 14 FPMD simulations were carried out (Figure 2, and Supporting Information, Figure S6). As found in the SMFS studies, the simulated unfolding F–D curves in most cases (12 of 14) showed two peaks per I27 unfolding. As the simulations used much faster pulling velocities (0.8  $\text{ms}^{-1}$ ) compared to SMFS (0.1–5  $\mu\text{m s}^{-1}$ ), the calculations revealed larger unfolding forces.

To determine the unfolding kinetics of I27, we performed dynamic SMFS (DFS), exposing the protein to different loading rates (Figure 3a, Supporting Information, Figure S1).

[\*] J. M. Nunes,<sup>[†]</sup> L. Ge, M. Lipinsky, Dr. J. Helenius, Prof. D. J. Muller  
Biotechnology Center, University of Technology  
01307 Dresden (Germany)

and

Department of Biosystems Science and Engineering, ETH Zurich  
4058 Basel (Switzerland)

Fax: (+41) 61-387-3994

E-mail: daniel.muller@bsse.ethz.ch

Dr. U. Hensen,<sup>[†]</sup> Prof. H. Grubmüller

Max-Planck-Institute of Biophysical Chemistry

37077 Göttingen (Germany)

Fax: (+49) 551-201-2302

E-mail: hgrubmu@gwdg.de

[†] These authors contributed equally to this work.

[\*\*] We thank Jane Clarke for supplying the I27<sub>8</sub> construct, C. Stange for assisting protein purification, and C. Bippes, K. T. Sagra, and J. Howard for discussions. The Max-Planck-Society, DFG, European Union, Fundação para a Ciência e Tecnologia, and Free State of Saxony supported this work.



Supporting information for this article is available on the WWW under <http://dx.doi.org/10.1002/anie.200906388>.

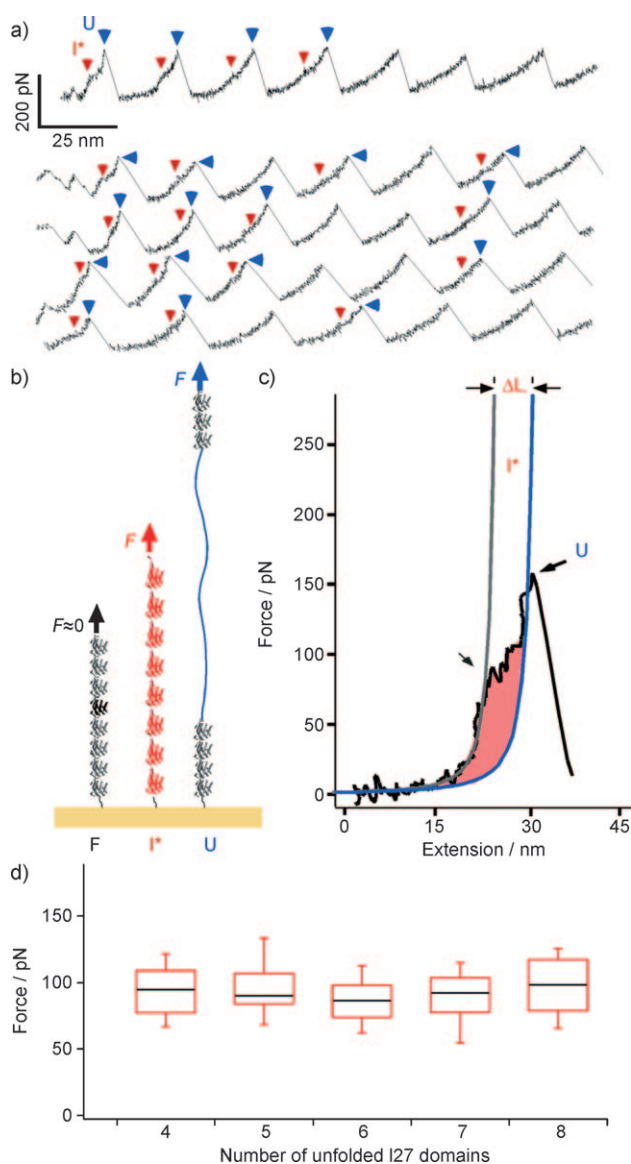


**Figure 1.** a) I27s unfold sequentially resulting in a sawtooth-like force–distance (F–D) curve. Arrowheads indicate the unfolding intermediate, I\* (red) and the complete unfolding of an I27, U (blue). The chance of detecting intermediate states decreases as the number of unfolded I27s increases. b) I27<sub>s</sub>, tethered to a gold support, pulled by an AFM cantilever. At approximately 95 pN all I27s unfold into an intermediate (I\*, red) before fully unfolding at higher force (U, blue). c) Force peaks were fitted using the worm-like chain (WLC) model to estimate the I\* (red) and U (blue) unfolding forces;  $\Delta L$  is the distance between unfolding intermediate (hump) and complete unfolding. d) Box plots of the forces (forces averages over all loading rates) that induced the first unfolding to the intermediate state with respect to number of Ig unfolding events in a I27<sub>s</sub> polymer (for 8, 7, 6, 5, and 4 Ig, the number of unfolding events  $n$  was  $n=84, 45, 37, 22,$  and  $30,$  respectively). Black lines represent medians, boxes comprise 50% of data, bars comprise values ranging from maximum to minimum.

The force at which the intermediate unfolded depended logarithmically on the loading rate  $l_r$ .<sup>[18]</sup> In contrast, the force at which fully folded Ig unfolded into the intermediate increased only slightly with loading rate.

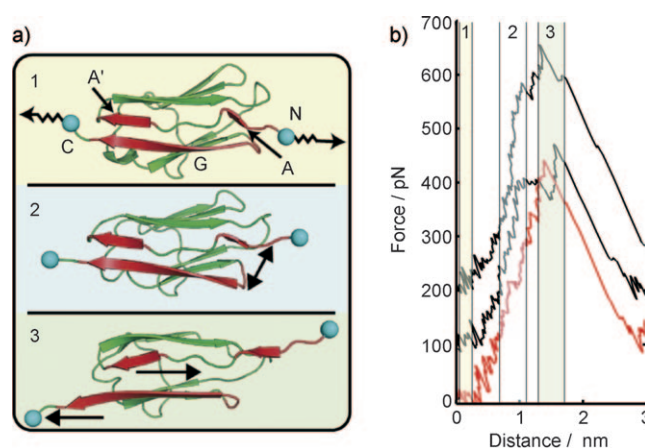


**Figure 2.** FPMD simulations of the force-induced unfolding of I27. a) Unfolding stages (1: folded, 2: intermediate, and 3: unfolded).  $\beta$ -strands A, A', and G are red. Harmonic spring potentials were applied to N- and C-terminal  $\alpha$  atoms (cyan balls) and retracted with constant velocity (black arrows in 1). b) F–D curves with (black) or without (red) unfolding via the intermediate state. The y values of the black curves were offset by 100 and 200 pN for better visibility. Background and numbers of the shaded areas correspond to the unfolding stages in (a). All simulations are shown in the Supporting Information, Figure S6.

FPMD and DFS data were then used to calculate kinetic rate constants and free-energy landscape. Unfolding rates at zero force  $k_{u,0}$  and rupture lengths  $x_u$  (Table 1) for both the transition into intermediate and the complete unfolding were obtained from 95% confidence intervals for linear least-square fits to the DFS data according to the Bell–Evans model (Figure 3a).<sup>[18]</sup> The graphical representation of the energy landscape (Figure 3b, purple) has two barriers, the heights of which are estimated from  $k_{u,0}$  and an attempt frequency of  $10^7 \text{ s}^{-1}$  (Supporting Information). The distance to the first barrier and that between both barriers was extracted from FPMD simulations. The distance between barriers could also be obtained experimentally by dividing  $\Delta L$  (Figure 1c) by the number of fully folded I27s.<sup>[8]</sup> As can be seen, the FPMD simulations and DFS measurements support each other.

To test whether the free-energy landscape obtained is consistent with the SMFS data beyond the Bell–Evans approximation, and also beyond the relatively short time scales accessible to atomistic simulations, we described the forced I27 unfolding with Brownian dynamics (BD) simulations obeying the Smoluchowski diffusion equation. In this approach, the end-to-end distance (extension) was used as a (diffusive) reaction coordinate subjected to a time-dependent two-barrier energy landscape (Supporting Information).<sup>[19]</sup> 11 300 BD simulations were performed with  $l_r$  values between  $10^6$  and  $10^{11} \text{ pNs}^{-1}$  (Figure 3a). Energy barrier positions, widths, and heights were adjusted iteratively until agreement with the least-squares fits of the DFS data was obtained. The spread of the BD forces agrees well with that expected from the force-induced crossing of a simple energy barrier (Supporting Information, Figure S7).<sup>[20]</sup> Though the same is found for the DFS regarding complete unfolding of I27, we obtain a

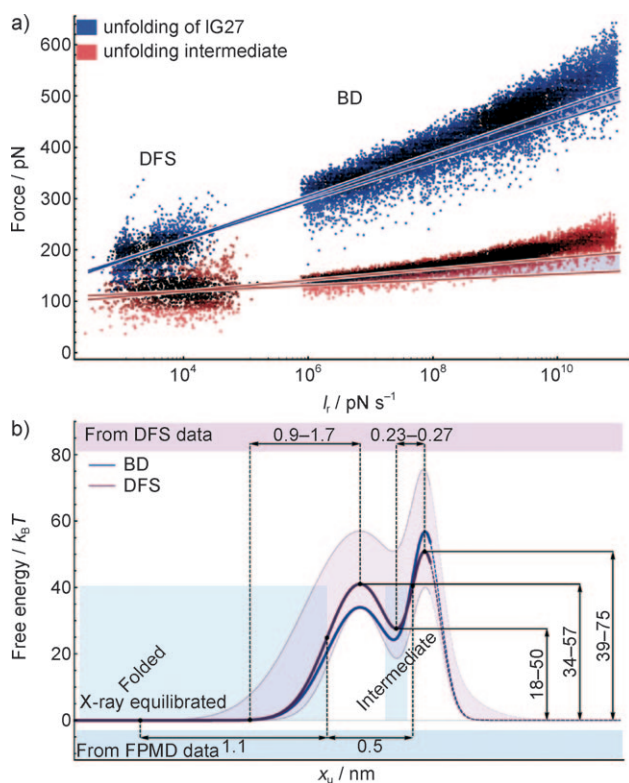


**Figure 3.** Kinetics of I27 unfolding. a) Dependence of I27 unfolding intermediate and unfolding force on loading rate  $l$ , (left: DFS measurement ( $n=4521$ ), right: BD simulation ( $n=11\,300$ )). Data are presented as density dots, with color intensity reflecting the frequency at which a certain force was detected (darker colors reflect higher density). Lines represent 95% confidence range of Bell–Evans model fits.<sup>[18]</sup> b) Free-energy landscapes of I27 unfolding derived from DFS measurements and FPMD simulations (purple shaded area from the error analysis of the fit to the DFS data, average as solid purple line) as well as BD potential matching of the DFS/FPMD data (blue line). Folded and intermediate states are indicated.

**Table 1:** Kinetic parameters describing the transitions between the folding states of I27 derived (see Supporting Information) from DFS measurements and FPMD and BD simulations.

Technique	Folded to intermediate			Intermediate to unfolded	
	$k_{u,0}$ [ $s^{-1}$ ]	$x_u$ [nm]	$k_f$ [ $s^{-1}$ ]	$k_{u,0}$ [ $s^{-1}$ ]	$x_u$ [nm]
DKS/FPMD	$1.3 \times 10^{-18}$ – $1.6 \times 10^{-8}$	0.9–1.7	$1600 \pm 51$	$4.1 \times 10^{-4}$ – $3.2 \times 10^{-3}$	0.23–0.27
BD	$1.7 \times 10^{-8}$	1.1	450	$3.7 \times 10^{-4}$	0.23

larger spread for the intermediate. We attribute this to the fact that the formation of the intermediate is difficult to locate in the AFM force traces, thus implying a larger error, especially for the later peaks.

The free-energy potential yielding the best agreement with the experimental results (Figure 3b, blue) largely matches the Bell–Evans potential derived from FPMD simulations (Figure 3b, purple). For additional comparison, kinetic rate constants were derived from this potential using the same attempt rate as above ( $10^7 s^{-1}$ ; Table 1). We conclude that this potential describes the free-energy landscape of I27 unfolding.

We investigated the structural changes associated with the intermediate state. In all the FPMD simulations, a rupture of hydrogen bonds between  $\beta$ -strands A and G (Figure 2a arrow in part 2) preceded the intermediate state. Subsequently, the hydrogen bonds between  $\beta$ -strands A' and G (Figure 2a red in part 3) ruptured at the main unfolding force peak. This rupture was followed by a sliding motion, which deformed the I27 structure (Figure 2a arrows in part 3). This result contrasts previous FPMD simulations which show that the mechanical unfolding of I27 begins with a rupture between  $\beta$ -strands A and B.<sup>[8,12]</sup> However, the earlier simulations used the NMR structure of an I27 mutant, in which some amino acids, such as I2 and T78 were replaced by others or were absent. Also, the hydrogen-bond network established between  $\beta$ -strands A and B is significantly tighter in the X-ray structure of wild-type I27 that we used.<sup>[17]</sup> This feature underscores the sensitivity of both unfolding path and force profile to small structural variations in I27 and, possibly, also to the lower loading rate used in our simulations. In agreement with our results, a force-distribution analysis indicates a prominent structural role of the interactions between  $\beta$ -strands A and G.<sup>[17]</sup>

A previous SMFS study on I27 unfolding suggests that an intermediate state occurs only at high loading rates<sup>[21]</sup> and, therefore, not under physiological conditions. However, our SMFS experiments indicate an unfolding intermediate in 95% of cases, even though the lowest pulling velocities closely resemble the mechanical stress in muscles. At the slowest experimental pulling velocity, the extension rate per folded protein length is  $2.5 s^{-1}$ . A sarcomere of  $2 \mu m$  length can contract at  $6 \mu m s^{-1}$ , yielding a contraction rate of  $3 s^{-1}$ .<sup>[22]</sup> The main unfolding force was the same whether an intermediate was present or not (5% of F–D curves; Supporting Information, Figure S4), suggesting that both I27 unfolding paths are the same. Indeed, in FPMD simulations the detachment of the  $\beta$ -strand A always precedes completing unfolding.

Our data suggests that the unfolding intermediate behaves as a “force buffer” considering its unusual independence from the loading rate (Figure 3a, Supporting Information, Figure S1). Clearly, this barrier creates a kinetic trap that significantly increases the lifetime of I27.

An association between the mechanics and topology of titin has been revealed. Mechanical properties of distal titin domains, such as I27, buffer the force: FPMD of I27 reveals that during unfolding the detachment of  $\beta$ -strand A forms an intermediate (Figure 2). This protection against high stretching forces increases with the number of domains in series.<sup>[8]</sup> Thus, titin has a stress absorbing capacity that prevents unfolding of Ig at forces that stress titin filaments in situ.<sup>[1,23]</sup> Our work contributes to the knowledge of how proteins establish bonds that resist mechanical stress. Normally, bonds resist an increasing applied force until the load reaches a threshold at which they then rapidly break. However, even small stressing forces

lower the energy barriers and shift the prevalent state towards the unbonded/unfolded state.<sup>[18]</sup> An exception are catch bonds that have longer lifetimes at certain loading rates.<sup>[24]</sup> The hydrogen-bond interactions of  $\beta$ -strand A with  $\beta$ -strands B and G of distal Igs are arranged in a way that within physiological pulling rates the energy barrier stabilizing the fully folded Igs remains fairly unaffected. Thus, the force required to overcome the barrier to the unfolding intermediate remains a constant. In distal Igs this system establishes a protection against unfolding. It remains to be shown in which other molecular systems such protective “force buffers” can be found as well as which roles they might have.

Received: November 12, 2009

Published online: March 30, 2010

**Keywords:** energy landscape · immunoglobulin · protein folding · scanning probe microscopy · titin

- 
- [1] L. Tskhovrebova, J. Trinick, *Nat. Rev. Mol. Cell Biol.* **2003**, *4*, 679.
- [2] W. A. Linke, M. Ivemeyer, P. Mundel, M. R. Stockmeier, B. Kolmerer, *Proc. Natl. Acad. Sci. USA* **1998**, *95*, 8052.
- [3] K. Wang, R. McCarter, J. Wright, J. Beverly, R. Ramirez-Mitchell, *Proc. Natl. Acad. Sci. USA* **1991**, *88*, 7101.
- [4] H. Li, W. A. Linke, A. F. Oberhauser, M. Carrion-Vazquez, J. G. Kerkvliet, H. Lu, P. E. Marszalek, J. M. Fernandez, *Nature* **2002**, *418*, 998.
- [5] L. Tskhovrebova, J. Trinick, *J. Biol. Chem.* **2004**, *279*, 46351.
- [6] S. Labeit, B. Kolmerer, *Science* **1995**, *270*, 293.
- [7] M. Rief, M. Gautel, F. Oesterhelt, J. M. Fernandez, H. E. Gaub, *Science* **1997**, *276*, 1109.
- [8] P. E. Marszalek, H. Lu, H. Li, M. Carrion-Vazquez, A. F. Oberhauser, K. Schulten, J. M. Fernandez, *Nature* **1999**, *402*, 100.
- [9] A. F. Oberhauser, P. K. Hansma, M. Carrion-Vazquez, J. M. Fernandez, *Proc. Natl. Acad. Sci. USA* **2001**, *98*, 468.
- [10] X. Zhuang, M. Rief, *Curr. Opin. Struct. Biol.* **2003**, *13*, 88.
- [11] M. Carrion-Vazquez, P. E. Marszalek, A. F. Oberhauser, J. M. Fernandez, *Proc. Natl. Acad. Sci. USA* **1999**, *96*, 11288.
- [12] M. Sotomayor, K. Schulten, *Science* **2007**, *316*, 1144.
- [13] S. B. Fowler, R. B. Best, J. L. Toca Herrera, T. J. Rutherford, A. Steward, E. Paci, M. Karplus, J. Clarke, *J. Mol. Biol.* **2002**, *322*, 841.
- [14] Y. Taniguchi, D. J. Brockwell, M. Kawakami, *Biophys. J.* **2008**, *95*, 5296.
- [15] H. Grubmüller, B. Heymann, P. Tavan, *Science* **1996**, *271*, 997.
- [16] B. Isralewitz, S. Izrailev, K. Schulten, *Biophys. J.* **1997**, *73*, 2972.
- [17] W. Stacklies, M. C. Vega, M. Wilmanns, F. Gräter, *Plos Comput. Biol.* **2009**, *5*, e1000306.
- [18] E. Evans, *Annu. Rev. Biophys. Biomol. Struct.* **2001**, *30*, 105.
- [19] S. Izrailev, S. Stepaniants, M. Balsera, Y. Oono, K. Schulten, *Biophys. J.* **1997**, *72*, 1568.
- [20] S. Koch, M. Wang, *Phys. Rev. Lett.* **2003**, *91*, 028103.
- [21] P. M. Williams, S. B. Fowler, R. B. Best, J. L. Toca-Herrera, K. A. Scott, A. Steward, J. Clarke, *Nature* **2003**, *422*, 446.
- [22] C. Opitz, M. Kulke, M. Leake, C. Neagoe, H. Hinssen, R. Hajjar, W. A. Linke, *Proc. Natl. Acad. Sci. USA* **2003**, *100*, 12688.
- [23] W. A. Linke, A. Grutzner, *Pflugers Arch.* **2008**, *456*, 101.
- [24] W. E. Thomas, V. Vogel, E. Sokurenko, *Annu. Rev. Biophys.* **2008**, *37*, 399.
-